Proceedings of the
International Conference on Mechanical Engineering 2011
(ICME2011) 18-20 December 2011, Dhaka, Bangladesh

ICME11-RT-011

STRUCTURAL, TRANSPORT AND DIELECTRIC PROPERTIES OF POLYCRYSTALLINE $Ca_{1-x}La_x(Ti_{0.5}Fe_{0.5})O_3$

M. R. Shah[1] and A. K. M. Akther Hossain[2]

[1] Department of Physics, Primeasia University, Banani, Dhaka, Bangladesh.
[2] Department of Physics, Bangladesh University of Engineering and Technology, Dhaka, Bangladesh.

ABSTRACT

Polycrystalline $Ca_{1-x}La_x(Ti_{0.5}Fe_{0.5})O_3$ are prepared by the standard solid state reaction technique and the samples are sintered at 1473 K for 5 hours in air. Structural formations are studied by X-ray diffraction and the XRD patterns of the samples indicate the formation of single phase orthorhombic structure. The bulk density and porosity of the sintered samples are measured by Archimedes principle. The lattice parameters as well as densities are increased but the average grain sizes are decreased with the increase of La content. The dielectric constant, loss tangent and ac conductivity are studied as a function of frequency for various compositions, and the behaviour is explained on the basis of Maxwell–Wagner model. The decrease of dielectric constant but improvement of dielectric losses is observed with the increase of La content in this study.

Keywords: X-Ray Diffraction, Dielectric Properties, Perovskite.

1. INTRODUCTION

Perovskite oxides of general formula ABO_3 have attracted much attention because of their wide range of technological applications such as multilayer capacitor, thermistors, varistors, energy converting systems, etc [1-5]. Some of ABO_3 oxides are exhibiting fascinating physical phenomena such as colossal magneto resistance, metal insulator transition and different transport mechanisms. $CaTiO_3$ with orthorhombic distortions of the perovskite structure was observed from X-ray diffraction by Naray-Szabo in 1943. It is paraelectric at room temperature, having dielectric permittivity above 180 and a dissipation factor (tanδ) $\sim 10^{-3}$ at 1 kHz [6]. Generally, the dielectric properties have been improved by suitable substitutions in the perovskite oxides [7-9]. There are three types of substitutions in the ABO_3. Substitutions may be performed at the A site, B site or both and these substitutions can be isovalent or heterovalent. Although extensive research works of the effect of isovalent substitutions on dielectric properties and transition temperatures of $CaTiO_3$ have been done during the last few decades but not much work has been done on the heterovalent substitutions [10-12].

Moreover, during the last few decade, most ABO_3 devices such as filters, resonators, actuators, sensors, and so on were prepared by using lead-based piezoelectric ceramic materials such as PTO, PZTO, PTSO etc [13-14]. These lead based ceramics have outstanding ferroelectric as well as dielectric properties. However, lead is a very toxic substance which can cause damage to the human health. Also, some countries have required all electronic products to be lead free for the protection of environment and human health. Therefore, with the recent growing demand of global environmental protection and human health, many researchers have greatly focused on lead-free ceramics to replace the lead-based ceramics [15-16]

With this view, La^{3+} substituted calcium titanate, $CaTiO_3$ with the formula $Ca_{1-x}La_x(Ti_{0.5}Fe_{0.5})O_3$ has been selected for studying of the structure and the dielectric properties.

2. EXPERIMENTAL

Various polycrystalline $Ca_{1-x}La_x(Ti_{0.5}Fe_{0.5})O_3$ (CLTFO) with $0.0 \leq x \leq 0.5$ compositions were prepared by the standard solid state reaction technique. Powders of $CaCO_3$ (99.9%), La_2O_3 (99.99%), TiO_2 (99.9%) and Fe_2O_3 (99.99%) were mixed thoroughly in stoichiometric amounts by ball milling in distilled water media for 10 hours. The slurry was dried and the mixed powders were calcined at 1223K for 12 hours in air. The calcined powders were re-milled for 10 hours and then dried. Finally, the dried powders were ground and from fine powders disk-shaped pellets with diameter of 0.01 m and thickness of 0.001-0.002 m were prepared under uniaxial pressure. The pellets were sintered at 1473 K for 5 hours. During sintering, the heating and cooling rates were maintained at 10 K/min and 5 K/min respectively.

The phase-purity and the crystal structure of the compositions were investigated by X-ray diffraction (XRD) with CuK_α radiation at room temperature. The bulk density, ρ_B, of the compositions was determined using the expression :

$$\rho_B = \frac{W}{W - W'} \times \rho$$

where W and W/ are the weights of the compositions in air and water respectively, and ρ is the density of water at room temperature. The theoretical density, ρ_{th}, was calculated using the expression:

$$\rho_{th} = \frac{4M_A}{N_A\, abc}$$

where N_A is the Avogadro's number (6.02×10^{23} mol^{-1}), M_A is the molecular weight and 'a, b and c' are the lattice parameters. The porosity, P, was calculated from the relation :

$$P(\%) = \frac{\rho_{th} - \rho_B}{\rho_{th}} \times 100$$

The surface morphology of sintered polished pellet was studied by a high resolution optical microscope (Olympus DP-70) and the average grain size was determined by the linear intercept technique [17].

In order to measure the dielectric properties, gold electrodes were deposited on both sides of the pellets and then gold wire was attached on each electrode with silver paste. The frequency dependence of the capacitance and the loss were measured by LCR meter at room temperature in the frequency range 10 Hz to 32 MHz. The dielectric constant, ε', was calculated from the capacitance using the equation:

$$\varepsilon' = \frac{Cd}{\varepsilon_0 A}$$

where C is the capacitance (F), ε_0 is the permittivity in free space, A is the area (m^2) of electrode and d is the thickness (m) of the pellet.

The ac conductivity, σ_{ac}, was calculated using room temperature dielectric data by the relation:

$$\sigma_{ac} = \varepsilon' \varepsilon_o \omega \tan\delta$$

where ω is the angular frequency and tanδ is the dielectric loss.

3. RESULTS AND DISCUSSION

3.1. Crystal Structure, Lattice Parameters and Density

Fig. 1 shows the XRD patterns for various CLTFO. The patterns indicate that all specimens are single phase perovskite and no second phases are detected. It implies that La^{3+} ions have entered into crystalline lattice structure to form a homogeneous solid solution. The XRD patterns for various CLTFO are in good agreement with an orthorhombic structure and the data have been indexed on the basis of orthorhombic symmetry [10, 12, 18]. It is also evident that the diffraction peaks of samples are shifted to the lower angle with the increase of La content. This may be due to the ionic radius of La^{3+} (1.36 Å) is higher than that of Ca^{2+} (1.34 Å) causes the increase of d spacing between the lattice [19].

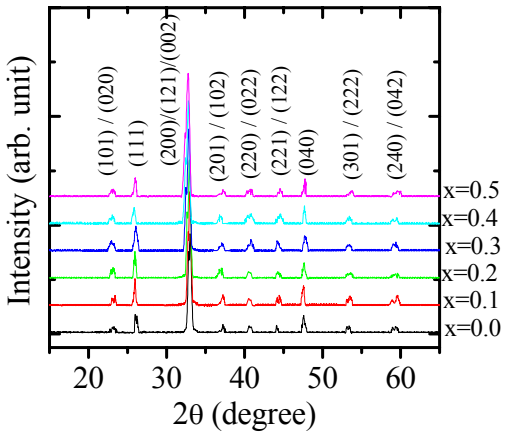

Fig 1. X-ray diffraction pattern of various polycrystalline $Ca_{1-x}La_x(Ti_{0.5}Fe_{0.5})O_3$ sintered at 1473 K.

Fig. 2 shows the variation of the lattice parameters a, b and c with La content for each compositions of CLTFO. It is observed from Fig. that the lattice parameters increase with the increase of La content. These variations can be explained on the basis of the ionic radii of the substituted cations as there is a correlation between the lattice parameters and ionic radius of the cations in the tetrahedral site. If the radius of the substituted cations is bigger than that of the displaced ions, the plane spacing is expanded and the lattice parameters are increased [20,21].The measured lattice parameters and crystal structure for different compositions are presented in Table 1.

Fig. 3 shows the variation of density and porosity of CLTFO as a function of La content. It is observed that the, ρ_B, increases and the corresponding, P, of the CLTFO compositions decreases with the increase of La content. The increase of density with the increase of La content may be attributed to the atomic weight and density of La (138.91 amu, 6.16×10^3 Kg/m^3) which are higher than those of Ca (40.00 amu, 1.55×10^3 Kg/m^3) [22]. Also, the replacement of Ca^{2+} by La^{3+} in the crystal leads to a variation in bonding and consequently inter-atomic distance and density. The oxygen ions which diffuse through the material during sintering also accelerate the densification of the material. It is also observed from Fig.3 that ρ_{th} is higher than ρ_B. This may be due to the existence of pores which are formed and developed

during the compositions preparation or the sintering process [23]. The ρ_{th} , ρ_B and P values of various CLTFO compositions are given in Table 1.

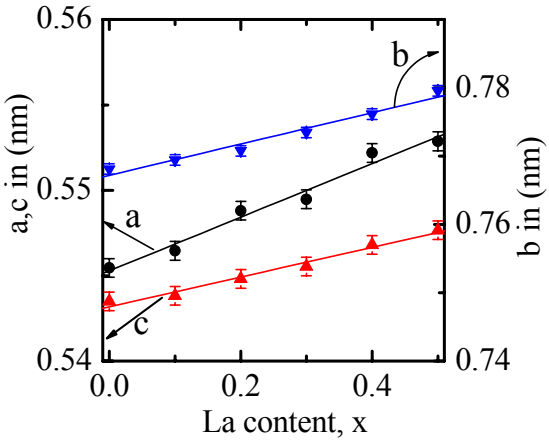

Fig 2. Variation of lattice parameters with La content of various $Ca_{1-x}La_x(Ti_{0.5}Fe_{0.5})O_3$ sintered at 1473 K.

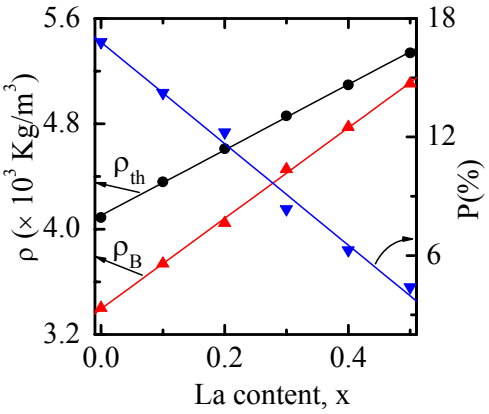

Fig 3. Variation of density and porosity with La content of various $Ca_{1-x}La_x(Ti_{0.5}Fe_{0.5})O_3$ sintered at 1473 K.

3.2. Microstructure

The optical micrographs of various CLTFO are shown in Fig. 4. The substitution of La has a significant effect on the grain size of the compositions. It is observed that the sintered CLTFO compositions are dense with the increase of La content. The average grain sizes for all compositions are presented in Table 1 and it is observed that the average grain size decreases from 4.41 μm to 0.84 μm with the increase of La content. The decrease of grain size may be due to the light weight Ca (40.00 amu) ions in the tetrahedral site are being replaced by the heavier weight of La (138.91 amu) ions which slower the diffusion process as a result of grain growth in CLTFO [24]. Also, the La has higher melting point (1193 K) than that of Ca (1115 K), it may be another reason the decrease of grain size with increase of La concentration.

Table 1: Lattice parameters, density, porosity and average grain size of $Ca_{1-x}La_x(Ti_{0.5}Fe_{0.5})O_3$ sintered at 1473 K.

x	Lattice parameters (nm)			ρ_{th} × 10^3 Kg/m^3	ρ_B × 10^3 Kg/m^3	P (%)	Grain Size (μm)
	a ±0.001	b ±0.001	c ±0.001				
0.0	0.5446	0.7667	0.5418	4.09	3.40	16.80	4.41
0.1	0.5457	0.7687	0.5421	4.36	3.74	14.23	3.03
0.2	0.5474	0.7701	0.5431	4.61	4.05	12.22	2.33
0.3	0.5498	0.7734	0.5441	4.86	4.46	8.34	1.77
0.4	0.5511	0.7754	0.5448	5.09	4.77	6.26	1.39
0.5	0.5525	0.7781	0.5458	5.34	5.10	4.38	0.84

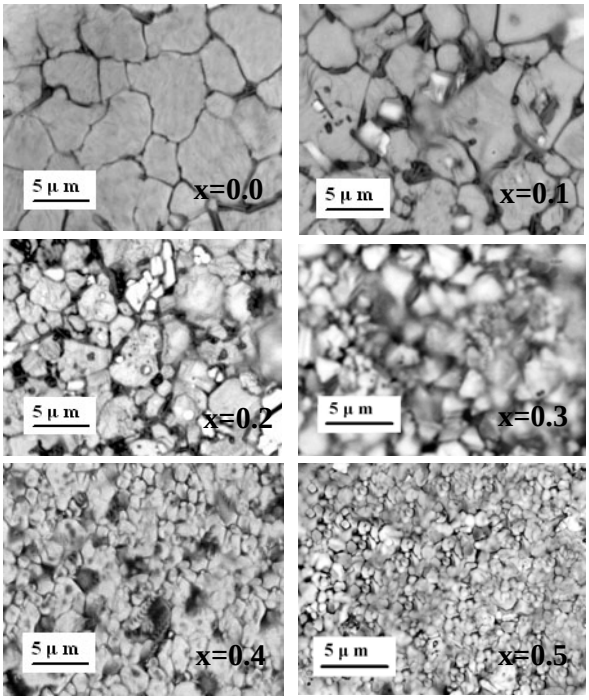

Fig 4. Optical micrographs of various $Ca_{1-x}La_x(Ti_{0.5}Fe_{0.5})O_3$ sintered at 1473 K.

3.3. Frequency dependence of dielectric constant ε′

Frequency dependence of the dielectric constant (ε') and dielectric loss (tanδ) for all samples studied at room temperature are shown in Fig. 5. It is clear from Fig. 5(a) that ε' has strong dependence on frequency in the lower frequency region and decrease with the increase in frequency. This variation of ε' with frequency can be explained on the basis of Maxwell-Wagner two layers model for spacecharge or interfacial polarization with Koop's phenomenological theory [25-27]. According to this model, dielectric materials are consist of large number of well conducting grains which are separated by poorly conducting thin grain boundaries. Under the application of external electric field, the charge carriers can easily migrate the grains but are accumulated at the grain boundaries. This process can produce large

polarization and high dielectric constant. The decrease of ε' with frequency arises from the fact that the polarization does not occur instantaneously with the application of the electric field because of inertia. The delay in response towards the applied alternating electric field leads to decrease in dielectric constant. Also, at lower frequencies, all four types' mechanism of polarization contributes to the total polarization of the material and hence higher value of dielectric constant. With the increase in frequency, the dipoles with large relaxation times cease to respond with the applied frequency and hence decrease in the dielectric constant. This type of frequency dependence dielectric behaviour is found in many ferroelectric materials [28-29].

3.4 Frequency dependence of dielectric loss (tanδ)

Fig. 5(b) shows the frequency dependence of the dielectric loss (tanδ) of the samples sintered at 1473K. It is clear from the Fig. that the samples show lower value of tanδ at lower frequency but it increases with the increase in frequency for all the compositions. Also, the loss is stable as well as fairly low up to the frequency about 7 MHz depends upon compositions. After that, at higher frequency, high dielectric dispersion of loss is observed due to some extrinsic loss phenomena. Several possible causes exist for such dispersion including the hypothesis of the influence of the contact resistance between the probe and electrode, presence of barrier layer between the insulating materials and the electrode surface, resonance due to high dielectric constant or leaky grain boundary. Similar frequency dispersion behaviour was also reported for other ferroelectric materials prepared by other techniques. [28].

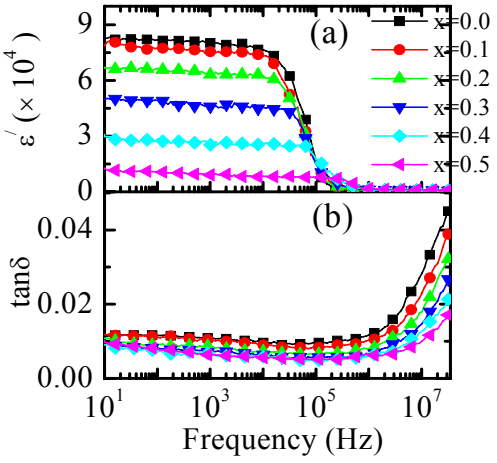

Fig 5. Frequency dependence of (a) dielectric constant (ε') and (b) dielectric loss (tanδ) of various $Ca_{1-x}La_x(Ti_{0.5}Fe_{0.5})O_3$ sintered at 1473 K.

3.5 Compositional dependence of dielectric constant ε′ and dielectric Loss (tanδ)

The variation of ε' and tanδ as a function of La content at different frequency for all samples are shown in Fig. 6.

The values of ε' decrease with the increase of La content as shown in Fig. 6 (a). This can be explained on the basis of Maxwell–Wagner theory. According to this theory the dielectric constant is directly proportional to the grain size of the samples [30]. The grain sizes of the samples decrease with the increase of La content as shown in the previous Fig. 4. The decrease in grain size leading to the decrease in polarizability of the atoms in the structure is reason for the decrease of dielectric constant.

The tanδ is found to decrease with the increase of La content as shown in Fig. 6 (b). This may be primarily attributed to the decrease in ε' with La substitution as well as increase in frequency. In general high permittivity materials possess higher losses.

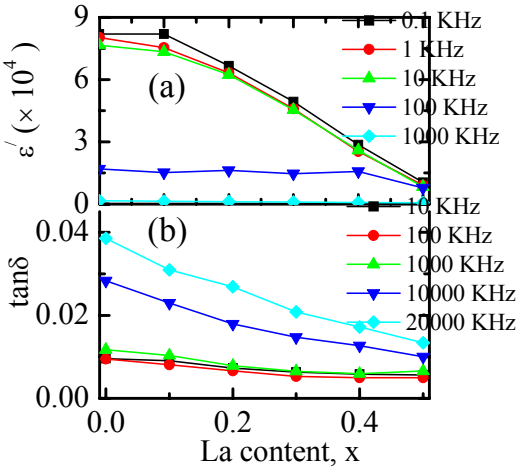

Fig 6. Compositions dependence of (a) dielectric constant (ε') and (b) dielectric loss (tanδ) of various $Ca_{1-x}La_x(Ti_{0.5}Fe_{0.5})O_3$ sintered at 1473 K.

3.6 Frequency dependence of ac conductivity

The ac conductivity of a system depends on the dielectric property and samples capacitance. This behaviour may be attributed to the presence of space charge in the material [31]. Usually, there are three effects that contribute to the ac conductivity: (i) the electrode effects are active at low frequency, (ii) the dc plateau is observed at intermediate frequencies and (iii) defect processes at higher temperature [32]. Fig. 7 shows the variation of ac conductivity of CLTFO as a function of frequency for all the compositions. The conductivity spectra display the typical shape found for an electronically conducting system. As shown in Fig. 7 that a plateau is observed in the 45 KHz to 7 MHz frequency region, i.e., a region where σ_{ac} is independent of frequency. Before and after this frequency range, the strong frequency dependent of σ_{ac} is observed. In the lower frequency region, the conductivity is strongly composition dependent and in the higher frequency it is independent of composition but only depend on frequency. So, high dielectric loss is observed in higher frequency region.

3.7 Compositional dependence of ac Conductivity

Fig. 8 shows the variation of ac conductivity as a function of compositions at different frequency. The conductivity is found to decrease with the increase of La content as well as increase in frequency. The decrease in conductivity may be primarily due to the decrease in loss with La substitution as stated earlier. Also, that decrease may be partly due to the decrease in grain size and hence increase in grain boundary areas or resistance with La. This increase of grain boundary resistance decreases the conductivity of the samples.

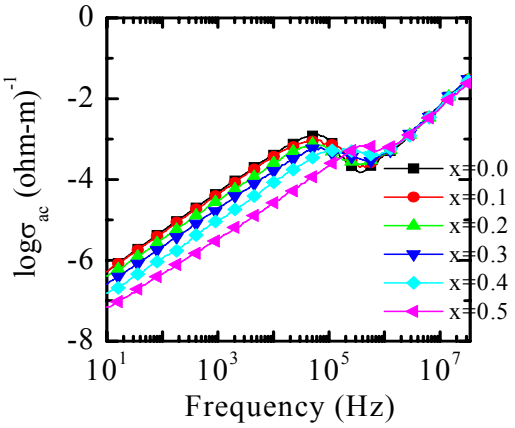

Fig 7. Frequency dependence of ac conductivity of various $Ca_{1-x}La_x(Ti_{0.5}Fe_{0.5})O_3$ sintered at 1473 K.

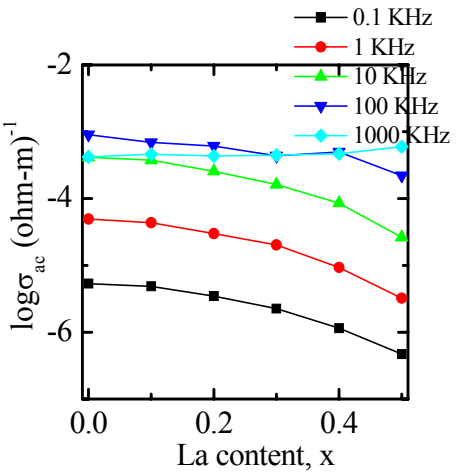

Fig 8. Compositions dependence of ac conductivity of various $Ca_{1-x}La_x(Ti_{0.5}Fe_{0.5})O_3$ sintered at 1473K.

4. CONCLUSIONS

The polycrystalline CLTFO are prepared by the standard solid state reaction technique. The XRD pattern of the samples shows the formation of single phase orthorhombic structure for all the samples. The lattice parameters and the density are found to increase but average grain sizes to decrease with the increase of La content. The dielectric properties of the samples strongly depend on the La concentration and microstructure. The data revealed that the dielectric constant decrease with the increase of La content and with frequency. The loss of the samples increases with frequency but decreases with the increase of La content due to decrease of grain size. The ac conductivity of the samples decreases as the decrease of loss of the samples.

ACKNOWLEDGEMENTS

The authors gratefully acknowledge CASR of Bangladesh University of Engineering and Technology (BUET) for financial support for this research.

5. REFERENCES

1. Haertling, G.. H., 1999, "Ferroelectric Ceramics: History and Technology", J. Am. Ceram. Soc, 82 (4) :797 - 818.
2. Jones, R. E., Mainar, P. D., Olowolafe, J. O., Campbell, J. O. and Mogab, C. J., 1992, "Electrical characteristics of paraelectric lead lanthanum zirconium titanate thin films for dynamic random access memory applications", Appl. Phys. Lett., 60 : 1022.
3. Cohen, R. E., 2000, "Theory of ferroelectrics: a vision for the next decade and beyond", J. Phys. Chem. Sol., 61 : 139- 146.
4. Kumar, M. M., Suresh, M. B., Suryanarayana, S. V., Kumar, G.. S. and Bhimasankaram, T., 1998, "Dielectric relaxation in $Ba_{0.96}Bi_{0.04}Ti_{0.96}Fe_{0.04}O_3$", J. Appl. Phys., 84: 6811 – 6814.
5. Settera, N., Damjanovic, D., Eng, L., Fox, G., Gevorgian, S., Hong, S., and et al., 2006, "Ferroelectric thin films: Review of materials, properties, and applications", J. Appl. Phys., 100: 051606.
6. Chung, C., Chang, Y. H., Chang, Y. S., and Chen, G. J., 2004, "High dielectric permittivity in $Ca_{1-x}Bi_xTi_{1-x}Cr_xO_3$ ferroelectric perovskite ceramics", J. Allo. Com., 385 : 298–303.
7. Patil, D. R., Lokare, S. A., Devan, R. S., Chougule, S. S., Kanamadi, C. M., Kolekar, Y. D. and Chougule, B. K., 2007, "Studies on electrical and dielectric properties of $Ba_{1-x}Sr_xTiO_3$", Mater. Chem. Phys., 104 : 254–257.
8. Singha, N. K., Kumara, P., and Raib, R., 2011, "Study of structural, dielectric and electrical behavior of $(1-x)Ba(Fe_{0.5}Nb_{0.5})O_3$–$xSrTiO_3$ ceramics", J. Allo.Com., 509: 2957–2963.
9. Rai, R., Sharma, S., Soni, N.C. and Choudhary, R.N.P., 2006, "Investigation of structural and dielectric properties of (La, Fe)-doped PZT ceramics", Physica B, 382 : 252–256
10. Ahmed, M. A. and Bishay, S. T., 2009, "Effect of annealing time, weight pressure and Fe doping on the electrical and magnetic behavior of calcium titanate", Mater. Chem. Phys., 114: 446–450.
11. Ramajo, L., Parra, R., Varela, J. A., Reboredo, M. M., Ramírez, M. A., and Castro, M.S., 2010, "Influence of vanadium on electrical and microstructural properties of

$CaCu_3Ti4O_{12}/CaTiO_3$", J. Allo. Com., 497: 349–353.
12. Chourasia, R., and Shrivastava, O. P., 2011, "Structure refinement of polycrystalline orthorhombic yttrium substituted calcium titanate: $Ca_{1-x}Y_xTiO_{3+\delta}$ (x = 0·1–0·3)", Bull. Mater. Sci., (Indian Academy of Sciences), 34 (1) : 89–95.
13. Ichinose, N., Miyamoto, N. and Takashi, S., 2004, "Ultrasonic transducers with functionally graded piezoelectric ceramics", J. Eur. Ceram. Soc., 24 : 1681- 1685.
14. Tressler, J.F., Alkoy, S. and Newnham, R. E., 1998, "Piezoelectric sensors and sensor materials", J. Electroceram, 2: 257 – 272.
15. Wang, Y., Yong-Xiang, L., Dong, W. and Qing-Rui, Y., 2006, "Relaxor behaviour and ferroelectric properties of $(Li_{0.12}Na_{0.88})(Nb_{0.9-x}Ta_{0.10}Sb_x)O_3$ Lead-Free Ceramics", Chin. Phys. Lett., 23: 2232 - 2235.
16. Du, H., Zhou, W., Luo, F. and Zhu D., 2007, "An approach to further improve piezoelectric properties of $(K_{0.5}Na_{0.5})NbO_3$-based lead-free ceramics", Appl. Phys. Lett. 91 : 202907 (1- 3).
17. Mendelson, M. I., 1969,"Average Grain Size in Polycrystalline Ceramics", J. Am. Ceram. Soc., 52 (8) : 443-46.
18. Wu, F., Zhang, Q. and Yang, H., 2009, "A general process to synthesize self-assembled shell-like $(Ca_{0.61}, Nd_{0.26})TiO_3$ clusters", J. Allo. Com., 488: 300–305.
19. Peng F., Xu Z., Chu R., Li W., Zang G. and Hao J., 2010, "Piezoelectric, ferroelectric and dielectric properties of Sm_2O_3-doped $(Bi_{0.5}Na_{0.5})_{0.94}Ba_{0.06}TiO_3$ lead-free ceramics", Mater. Chem. Phys., 124: 1065–1070.
20. Cavalcante, L.S., SimÕes, Espinosa, J.W.M., Santos, L.P.S., Longob, E., Varela, J.A., and Pizani, P.S., 2008, "Study of structural evolution and photo luminescent properties at room temperature of $Ca(Zr,Ti)O_3$ powders", J. Allo. Com., 464: 340–346.
21. Chung, C. Y., Chang, Y.H. and Chen, G. J., 2004 , "Effects of lanthanum doping on the dielectric properties of $Ba(Fe_{0.5}Nb_{0.5})O_3$ ceramic", J. Appl. Phys., 96 (11): 6624 – 6628.
22. Abdeen, A.M., Hemeda, O.M., Assem, E.E., and El-Sehly, M. M., 2002,"Structural, electrical and transport phenomena of Co ferrite substituted by Cd", J. Magn. Magn. Mater., 238: 75–83.
23. Mahmud, S.T., Akther Hossain, A.K.M., Abdul Hakim, A.K.M., Seki, M., Kawai, T. and Tabata, H., 2006 "Influence of microstructure on the complex permeability of spinel type Ni–Zn ferrite", J. Magn. Magn. Mater., 305 : 269–274..
24. Zhang, J., Zhai J., Chou, X., and Yao, X., 2008, "Influence of rare-earth addition on microstructure and dielectric behavior of $Ba_{0.6}Sr_{0.4}TiO_3$ ceramics", Mater. Chem. Phys., 111 : 409–413.
25. Maxwell, J. C., 1973, "*Electricity and Magnetism*", Vol 1, Oxford, Oxford University Press, (1929).
26. Wagner, K. W., 1973, Am. Phys. 40 : 317.
27. Koops, C. G., 1951, "On the dispersion of resistivity and dielectric constant of some semiconductors at audio frequencies", Phys. Rev., 83: 121-124.
28. Patil, D. R., Lokare, S. A., Devan, R. S., Chougule, S. S., Kanamadi, C.M., Kolekar, Y. D., and Chougule, B. K., 2007, "Studies on electrical and dielectric properties of $Ba_{1-x}Sr_xTiO_3$", Mater. Chem. Phys. 104: 254–257.
29. Verma, K. C., Ram, M., Singh, J., and Kotnala, R. K., 2011, "Impedance spectroscopy and dielectric properties of Ce and La substituted $Pb_{0.7}Sr_{0.3}(Fe_{0.012}Ti_{0.988})O_3$ nanoparticles", J. Alloy. Com., 509: 4967–497.
30. Shah, D. D., Mehta, P. K., Desai, M..S., and Panchal, C. J., 2011,"Origin of giant dielectric constant in $Ba[(Fe_{1-x}Co_x)_{1/2}Nb_{1/2}]O_3$", J. Allo. Com., 509 : 1800–1808.
31. Singh, N.K., Kumar, P., and Rai, R., 2011, "Study of structural, dielectric and electrical behavior of $(1-x)Ba(Fe_{0.5}Nb_{0.5})O_3–xSrTiO_3$ ceramics", Alloy. Com., 509: 2957–2963.
32. Shukla, A. Choudhary, R.N.P. and Thakur, A.K., 2009, "Thermal, structural and complex impedance analysis of Mn^{4+} modified $BaTiO_3$ electroceramic", J. Phys. Chem. Sol., 70 : 1401–1407.

6. NOMENCLATURE

Symbol	Meaning	Unit
A	Area of electrode	(m^2)
a,b,c	Lattice parameters	(Å)
C	Capacitance	(Farad)
d	Thickness of the plate	(m)
N_A	Avogadro's number	($mole^{-1}$)
ρ_B	Bulk density	(kg/m^3)
ρ_{th}	Theoretical density	(kg/m^3)
P	Porosity	Unit less
ε_0	Permitivity in free space	$C^2/N.m^2$
ε'	Real part of Dielectric constant	Unit less
σ_{ac}	AC conductivity	$(Ohm\text{-}m)^{-1}$
T	Temperature	(K)
tanδ	Dielectric loss	Unit less

7. Mailing Address
M. R. Shah
Department of Physics,
Primeasia University, Banani, Dhaka, Bangladesh
E-mail:hirubd@yahoo.com